PAPER • OPEN ACCESS

Electrically switchable metasurface for beam steering using PEDOT polymers

To cite this article: Juliane Ratzsch *et al* 2020 *J. Opt.* **22** 124001

View the article online for updates and enhancements.

Electrically switchable metasurface for beam steering using PEDOT polymers

Juliane Ratzsch[1]**, Julian Karst**[1] **, Jinglin Fu**[1]**, Monika Ubl**[1]**, Tobias Pohl**[1]**, Florian Sterl**[1] **,
Claudia Malacrida[2]**, Matthias Wieland**[2]**, Bernhard Reineke**[3]**, Thomas Zentgraf**[3] **,
Sabine Ludwigs[2] **, Mario Hentschel**[1] **and Harald Giessen**[1]

[1] 4th Physics Institute and Research Center SCoPE, University of Stuttgart, Pfaffenwaldring 57, 70569
Stuttgart, Germany
[2] IPOC-Functional Polymers, Institute of Polymer Chemistry, University of Stuttgart, Pfaffenwaldring 55,
70569 Stuttgart, Germany
[3] Department of Physics, Paderborn University, 33098 Paderborn, Germany

E-mail: h.giessen@pi4.uni-stuttgart.de

CrossMark

Abstract
Switchable and active metasurfaces allow for the realization of beam steering, zoomable
metalenses, and dynamic holography. To achieve this goal, one has to combine
high-performance metasurfaces with switchable materials that exhibit high refractive index
contrast and high switching speeds. In this work, we present an electrochemically
switchable metasurface for beam steering where we use the conducting polymer
poly(3,4-ethylenedioxythiophene) as an active material. We show beam diffraction with angles
up to 10° and a change of the intensities of the diffracted and primary beams employing an
externally applied cyclic voltage between -1 V and $+0.5$ V. With this unique combination, we
realize switching speeds in the range of 1 Hz, and the extension to typical display frequencies in
the region of tens of hertz is possible. Our findings have immediate implications for the design
and fabrication of future electronically switchable and display nanotechnologies, such as
dynamic holograms.

(Supplementary material for this article is available online)

Keywords: nanooptics, plasmonics, switchable metasurface, PEDOT, electrochemistry,
beam steering

(Some figures may appear in colour only in the online journal)

1. Introduction

The manipulation of optical wavefronts via lenses, mirrors, or any other optical devices is present in our everyday lives. This includes bulky lenses made from glasses, Fresnel lenses in smartphone illumination optics, and spatial light modulators and liquid crystals in displays. However, emerging display technologies such as dynamic holography or augmented and virtual reality require ever-increasing pixel densities and thus new smart optical methods with the ability to manipulate optical wavefronts, beam paths, polarization, and similar activities on ultra-small length scales [1–3]. To meet this demand, there has been a significant increase in interest in the research field of plasmonics over the last years as plasmonic nanoparticles allow one to focus, manipulate, or steer

light on the nanometer scale at subwavelength dimensions [4–6]. The combination of optically active and externally switchable materials with plasmonics into hybrid nanosystems has increased their applicability even further and opened the door towards active plasmonically driven light manipulation [7]. Plasmonic metasurfaces that are artificial sheet materials with sub-wavelength thickness are particularly good at allowing the realization of flat optical components with unique optical properties [8–13]. Furthermore, the combination with phase change materials enables active plasmonic optical applications such as active beam switching [14, 15], zoom lensing [16], dynamic holography [17], dynamic plasmonic color displays [18, 19] and many more. One possibility to realize these hybrid nanosystems is the fabrication of nanoparticles directly from phase change materials such as magnesium [20–23], palladium [24–27], and yttrium [28]. Additionally, phase change materials such as polyaniline [29, 30], germanium–antimony–tellurium-based films (GST) [31–34], liquid crystals [35, 36], or VO_2 [37, 38] are widely used in combination with nanoparticles to allow for active switching. However, widespread and commercial applications have so far been hindered by several limiting factors such as material degradation, slow switching speeds, low optical contrast (refractive index shifts). Even more, most material phase transitions are only accessible via variations in, for example, temperature or exposed gases and not electrically.

Here, we present an optically active system to perform switchable beam steering realized via a novel hybrid metasurface. It consists of a unique combination of gold plasmonic nanoantennas and the electrically switchable and conducting polymer poly(3, 4-ethylenedioxythiophene) (PEDOT) [39, 40]. We show that tuning of geometric parameters allows for switching angles and beam diffraction of up to 10°, while the efficiency of the hybrid metasurface and thus the intensity of diffracted light can be actively controlled via an externally applied cyclic voltage between only −1 V and +0.5 V. An increase of the scan rate of the cyclic voltammetry reveals switching frequencies close to 1 Hz, while an extension to typical display frequencies in the range of tens of hertz is possible, only limited by the measurement components.

2. Experimental details

In order to design the plasmonic nanostructures, we used the transient solver of CST Microwave Studio Suite in a wavelength range between 600 nm and 1200 nm. Figure 1(a) shows the material stack and geometries of the simulated system. We simulated a single unit-cell with open boundary conditions in the *z*-direction to emulate free space and periodic boundary conditions in the *x*-direction and *y*-direction to simulate an infinite array of antennas. To optimize the on/off behavior, we performed two simulations—one series with the refractive index of the reduced PEDOT and one sequence with the oxidized PEDOT. With a parameter scan, the geometry was optimized to find an antenna geometry, which leads to a significant shift of the plasmonic resonance when the refractive index of the PEDOT changes. The resulting
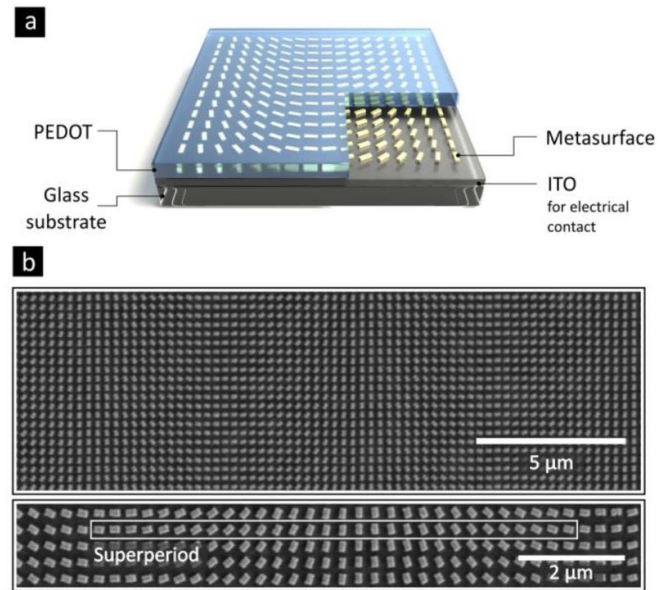

Figure 1. (a) Schematic of the active plasmonic metasurface for beam steering. Gold nanoantennas on an ITO covered glass substrate, coated with electropolymerized PEDOT, which act as the reversibly switchable layer (refractive index shift) during cyclic voltammetry. ITO is used for electrical contact. (b) SEM image of the metasurface. The super period, consisting of 30 antennas, is marked in white in the lower zoom-in image.

amplitude and phase spectra of the transmission coefficient for cross- and co-polarization can be found in figure S1 (available online at https://stacks.iop.org/JOPT/22/124001/mmedia) in the supplementary information. The resonance shift allows us to turn on and off the anomalous refraction of the plasmonic antenna array at a specific wavelength. The refractive index of PEDOT was taken from Stockhausen *et al* [39]. Further, the refractive index of gold was taken from Yakubovsky *et al* [41].

The final metasurface consists of gold nanoantenna arrays with progressively rotated elements along one axis [42], as shown in the SEM images in figure 1(b). Fabrication is done via electron-beam lithography (Raith eLine Plus). The antennas have a size of 200 × 135 nm, a thickness of 50 nm, and a period of 300 nm in the *x*-direction and *y*-direction and are placed on a glass substrate covered with a thin layer (20 nm) of indium–tin–oxide (ITO) for electrical contact. Adjacent antennas are rotated with an incremental rotation angle of 6°. The resulting super period after 180° rotation is 9 μm and comprises 30 antennas, as marked in the lower SEM image in figure 1(b). When illuminating this metasurface with the circularly polarized light of one handedness, the design results in an additional transmitted beam that is diffracted from the main beam by several degrees and possesses opposite circular polarization. To make our hybrid metasurface electrically switchable in the visible spectral range, we cover the metasurface with a 150–200 nm thick PEDOT layer which is deposited by electropolymerization [43, 44]. This PEDOT layer undergoes a significant refractive index change in the visible spectral range when the applied voltage is varied by cyclic

voltammetry [45] and thus results, in combination with the metasurface, in electrochemically activated switchable beam steering. Please note that modifying the deflection angles or similar would require an active change of the metasurface parameters (antenna geometry, spacing, etc) or the combination of multiple metasurfaces. So far, this is not possible with our hybrid metasurface design. See figure S2 in the supplementary information for details on the electrodeposition and structural change of PEDOT.

A schematic drawing of our main setup used to perform angle-resolved imaging is shown in figure 2(a). It consists of a modified transmission microscope (Nikon Eclipse TE2000-U) in combination with a home-built k-space imaging module [27]. We use a tunable laser (NKT Photonics SuperK Extreme) as an illumination source, set at a wavelength of $\lambda = 750$ nm. To obtain right-circularly polarized light we use a polarizer (Thorlabs LPVIS100) and a broadband quarter-wave plate (QWP) (B. Halle RAC 5.4.20). As we image in k-space, the condenser is set highly defocused to allow for the best possible normal incidence on the metasurface. The metasurface is placed at the sample position in the front focal plane of the objective (Nikon Plan Fluor ELWD 40x, N.A. 0.60), which collects the main transmitted and the diffracted beam. The diffracted beam is left-circularly polarized and thus possesses the opposite circular polarization compared to the main beam. Consequently, a circular analyzer consisting of another QWP (B. Halle RAC 5.4.20) and polarizer (Thorlabs LPVIS100) allows for the adjustment of the intensity of two beams. As the main beam is more intense in our experiments, we use this circular analyzer to attenuate the main beam, resulting in similar intensities of both beams before starting the switching experiment. To be able to resolve the diffraction angles of the two beams, we directly image the objective back focal plane (k-space) with a modified 4-f setup [46] on a charge-coupled device (CCD) camera (Allied Vision GC2450C). As schematically depicted in figure 2(a), the sample is placed inside a custom-made electrochemical cell to perform cyclic voltammetry on the active PEDOT layer with a three-electrode setup. A schematic drawing of the electrochemical setup is shown in figure 2(b). As the electrolyte, we use a 0.1 mol l^{-1} CH_3CN/Bu_4NPF_6 solution. We attach the working electrode (platinum (Pt) wire) to the electrically conducting and partially uncovered ITO layer underneath the metasurface. The counter electrode (Pt wire) and reference electrode (silver chloride silver wire, Ag/AgCl) are in contact with the electrolyte solution. The reference electrode is placed near the working electrode to minimize Ohmic drops of the voltammogram. Finally, the three electrodes are connected to a potentiostat (BioLogic SP-200) to perform cyclic voltammetry between -1 V and $+0.5$ V vs. Ag/AgCl. The typical voltammogram of the PEDOT deposited on our metasurface and a ferrocene reference are shown in figure S2 in the supplementary information.

3. Results and discussion

The effect of beam steering is obtained via the refractive index shift of the PEDOT layer during cyclic voltammetry.
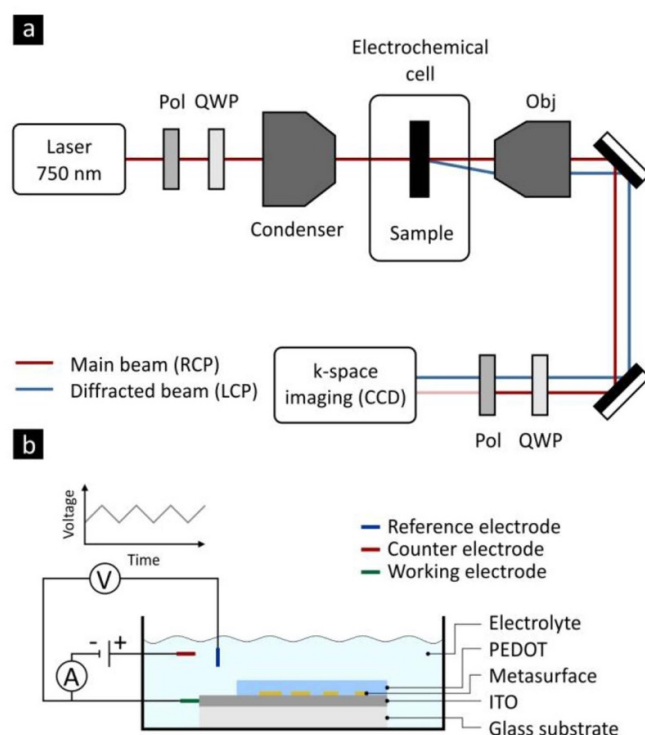

Figure 2. (a) Schematic of the k-space setup used to measure the diffraction of the actively switchable metasurface. The main incident beam is right-circularly polarized (RCP), while the diffracted beam is left-circularly polarized (LCP). The circular analyzer (second pair of QWP and Pol) allows for diminishing the main beam. (b) Schematic of the electrochemical cell where the PEDOT is actively switched via cyclic voltammetry.

This change in the refractive index causes the plasmonic resonance of the metasurface to shift and thus the efficiency of the beam diffraction to vary. The spectral response of our hybrid metasurface is shown in figure 3(a). For spectral measurements, we replace the k-space imaging module in figure 2(a) with a grating spectrometer (Princeton Instruments SP2500i) and a Peltier-cooled front-illuminated CCD camera (Acton PIXIS 256E). In the oxidized state (red curve), we find a broad plasmonic resonance with a centroid wavelength around $\lambda_{c,O} = 760$ nm. In contrast, the plasmonic resonance in the reduced state (blue curve) is red-shifted by approximately 85 nm to a centroid wavelength around $\lambda_{c,R} = 845$ nm. Overall, this matches the spectral shift expected from the refractive index shift of PEDOT [43, 45]. Furthermore, a spectral transmission peak around $\lambda = 720$ nm is found in the reduced state. This peak originates from the overlay of the plasmonic resonance dip at $\lambda_{c,R} = 845$ nm and the intrinsic PEDOT material transmission dip (absorption peak) around $\lambda = 600$ nm. This material resonance is also visible in the transmission spectra of only the electropolymerized PEDOT layer in the oxidized and reduced states, which can be found in figure S3 in the supplementary information. The temporal behavior of the centroid wavelength during cyclic voltammetry is depicted in figure 3(b). The upper graph shows the centroid wavelength versus time for a total of four cycles. The centroid wavelengths are determined from the spectral responses of the metasurface from figure 3(a). Centroids of the metasurface in the reduced
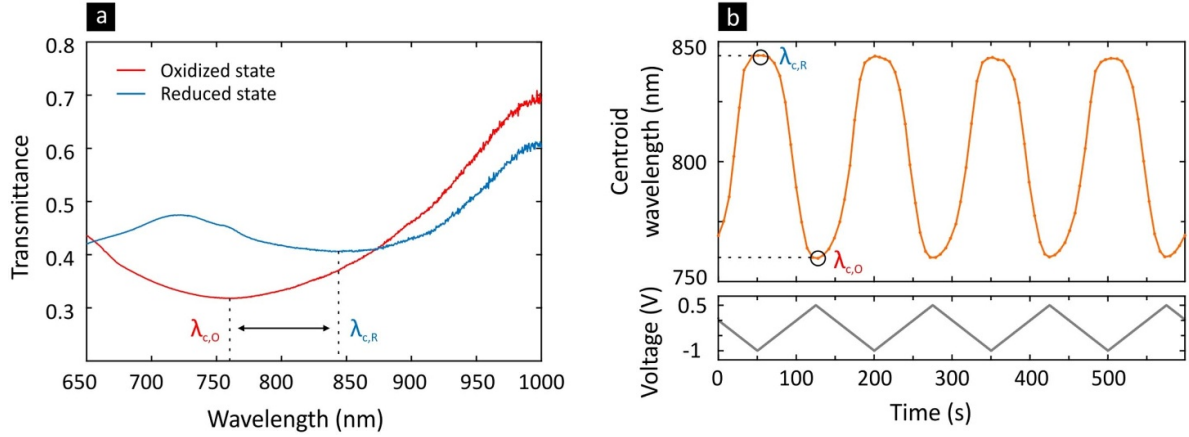
Figure 3. Spectral shift of the plasmonic resonance of the hybrid metasurface. (a) Transmittance of the metasurface in the oxidized state (red) and reduced state (blue) of PEDOT at the extrema during cyclic voltammetry (oxidized and reduced PEDOT). (b) Centroid wavelength and applied voltage over time. The voltage is measured versus a Ag/AgCl pseudoreference electrode. Marked are $\lambda_{c,O}$ of the oxidized state and $\lambda_{c,R}$ of the reduced state of PEDOT.

state ($\lambda_{c,R}$) and the oxidized state ($\lambda_{c,O}$) are marked in blue and red, respectively. The lower graph in figure 3(b) depicts the voltage cycling between -1 V and $+0.5$ V with a scan rate of 20 mV s^{-1}. We find that the centroid wavelength cycles between the oxidized and reduced states and that the PEDOT and thus the hybrid metasurface respond immediately to changes in the voltage. The reduced and oxidized states are separated from each other, which allows for stable cycling between the two distinct optical states. Furthermore, the switching is reproducible over several cycles with no indication of any degradation.

As our hybrid metasurface is designed to allow for switchable beam steering in the visible spectral range, we now turn our attention to angle-resolved k-space imaging, as illustrated in figure 4. The beam profiles and intensities of the zeroth-order main and first-order diffracted beam in k-space are illustrated in figures 4(a) and (b) for the oxidized and reduced states, respectively (illumination wavelength $\lambda = 750$ nm). The lower graphs depict the spatially resolved intensity in k-space, whereas the upper graphs show the corresponding integrated intensities. Overall, we find a Gaussian beam profile of both beams. Please note that the intensities are obtained by converting the CCD camera images from sRGB to linear RGB. In the oxidized state in figure 4(a), the diffracted beam I_1 has a higher intensity in comparison to the main beam I_0. In contrast, this relation inverts for the reduced state in figure 4(b), as here the diffracted beam has a lower intensity than the main beam. We find that the total intensity of both beams increases, which results from the overall higher transmittance of the hybrid metasurface in the reduced state at $\lambda = 750$ nm (compare to figure 2(a)). The diffraction of this designed hybrid metasurface in k-space is $k_x = \sin \theta_x = 0.085$, which corresponds to a diffraction angle of $\theta_x = 4.9°$. By changing the super period of the metasurface, we can increase the diffraction angle to $\theta_x \approx 10°$. The k-space and temporal response that depend on the applied voltage of this modified metasurface are shown in figure S4 in the supplementary information.

For potential applications as light modulators, it is important to determine the modulation efficiency of our metasurface. In detail, we determine two quantities necessary to quantify our metasurface relative to the existing literature. The first parameter, the basic efficiency,

$$\eta^{\mathrm{ox}} = \frac{I_1^{\mathrm{ox}}}{I_0^{\mathrm{ox}}/a},$$

is calculated via the intensity ratio of the diffracted beam I_1^{ox} and the main beam I_0^{ox} in the oxidized PEDOT state. Please note that we introduce and experimentally determine the attenuation coefficient a, which originates from the attenuation of the main beam I_0 via the QWP (see figure 2(a)). Consequently, we obtain the efficiency values of the metasurface in figure 4 of $\eta^{\mathrm{ox}} = 3.67\%$. The efficiency of the modified metasurface in figure S4 is $\eta^{\mathrm{ox}} = 0.83\%$.

A second quantity to compare is the figure of merit [47]:

$$\mathrm{FOM} = \frac{1}{2}\left(C^{\mathrm{ox}} - C^{\mathrm{red}} \right) = \frac{1}{2}\left(\frac{I_0^{\mathrm{ox}}/a - I_1^{\mathrm{ox}}}{I_0^{\mathrm{ox}}/a + I_1^{\mathrm{ox}}} - \frac{I_0^{\mathrm{red}}/a - I_1^{\mathrm{red}}}{I_0^{\mathrm{red}}/a + I_1^{\mathrm{red}}} \right),$$

where $I_1^{\mathrm{ox}}, I_1^{\mathrm{red}}$, and $I_0^{\mathrm{ox}}, I_0^{\mathrm{red}}$ are the intensities of the diffracted and main beam in the oxidized and reduced states, respectively. C^{ox} and C^{red} denote the contrasts in the oxidized and reduced states, respectively. A complete transfer of the intensity from the main beam to the diffracted beam during switching would result in FOM $= 1$. For our metasurface in figure 4, we obtain a value of FOM $= 0.05$, whereas for the modified metasurface in figure S4 we obtain FOM $= 0.01$. These values are small compared to other active metasurface designs in the literature [47], which most likely originates from the comparably small refractive index shift of PEDOT in the visible spectral range.

The intensity ratio I_1/I_0 of our initial metasurface during cyclic voltammetry is plotted in figure 4(c). Please note that due to the reduced intensity of the main beam I_0, the
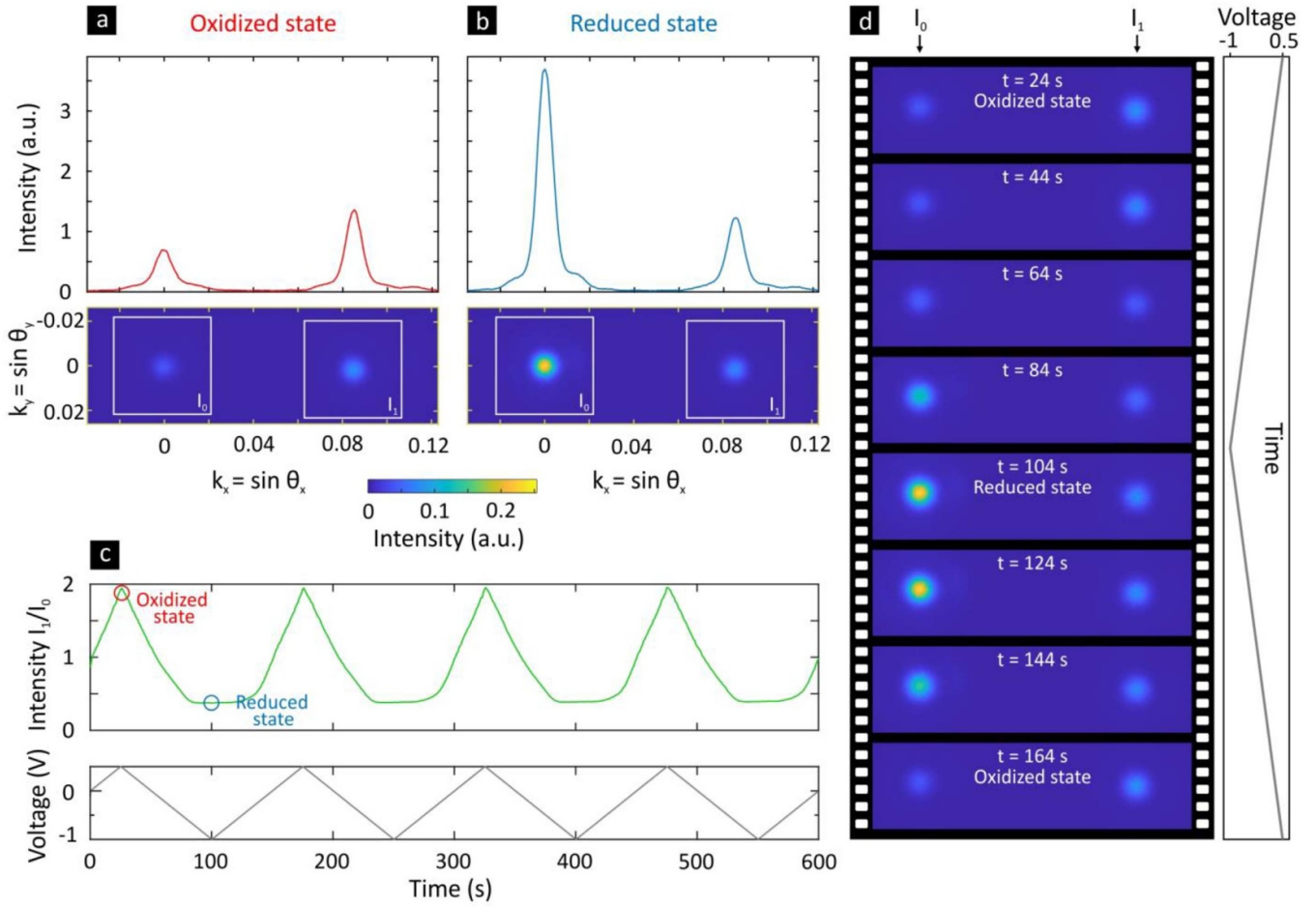
Figure 4. (a), (b) Intensity captured by the CCD camera in k-space (lower image panels) and integrated intensity profiles (upper panels) for the reduced and oxidized states, respectively, displaying the zeroth-order beam and first-order diffracted beam. (c) Contrast (intensity ratio I_1/I_0 of the first- and zeroth-order beams) during cyclic voltammetry (tuning of the applied voltage). The areas of the respective beam sizes for the intensity calculation are shown with white frames in (a) and (b). (d) Intensity captured by the CCD camera during one cycle. A video showing all frames can be found in the supplementary information. The illumination wavelength is $\lambda = 750$ nm.

absolute value of the intensity ratio I_1/I_0 is in fact smaller, as we discussed above for the calculation of the efficiency of the metasurface. A further increase of the intensity ratio and thus diffraction efficiency might be possible by considering other metasurface designs with modified design parameters (metasurface material, antenna geometry, operating wavelength, variation of active material, and many more). Again, we find that the hybrid metasurface quickly reacts to voltage changes. In the oxidized state after $t = 24$ s, the ratio has a sharp maximum, whereas in the reduced state after $t = 104$ s we find a flat plateau around the minimum. The observed temporal behavior of the intensity ratio clearly shows that we can actively control the intensity of both beams. The intensities of the individual beams during cyclic voltammetry are plotted in figure S5 in the supplementary information. The variations in the beam intensities do not originate from a simple transmittance change of the PEDOT, which would result in a temporal constant intensity ratio I_1/I_0, but rather from a change in the diffracted intensity due to its refractive index change and subsequent tuning of the metasurface plasmonic resonance. We find from the individual beam

intensities in figure S5 that it is, in fact, possible to vary the diffracted beam intensity individually while the intensity of the main beam remains constant. Thus, the 'gained' intensity in the diffracted beam needs to result in a reduced intensity in higher-order beams and background (mostly diffuse scattering). Consequently, we are able to vary the diffraction efficiency of the hybrid metasurface via the applied voltage. Selected k-space images of this beam steering process are depicted in figure 4(d). A video showing all frames can be found in the supplementary information. The positions of the main (I_0) and diffracted beams (I_1) are marked with arrows. We observe the switching behavior of the metasurface cycling between higher intensity in the diffracted beam and higher intensity in the main beam.

For practical applications in active and zoomable lens designs or future display technologies, active metasurfaces ideally should have switching speeds at typical display frequencies in the range of tens of hertz. Consequently, as a final step we investigate the response and switching time of our hybrid metasurface by varying the scan rate during cyclic voltammetry. The results are depicted in figure 5 for scan rates
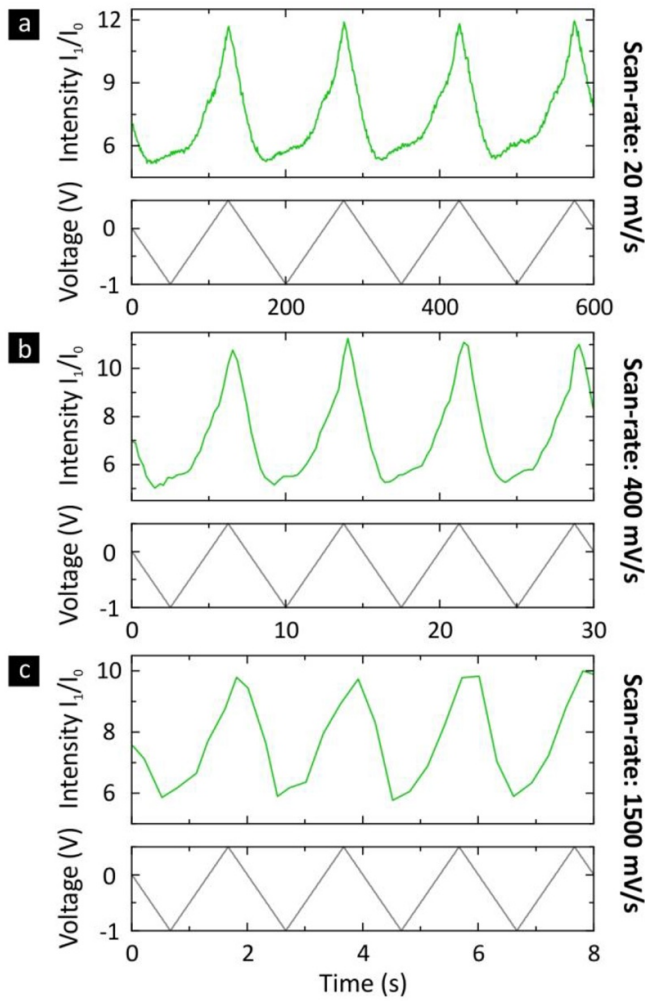
Figure 5. Response of the metasurface for the different scan rates of (a) 20 mV s^{-1}, (b) 400 mV s^{-1}, and (c) 1500 mV s^{-1}. The upper graphs depict the ratio I_1/I_0 of the intensity of the diffracted beam I_1 and the main beam I_0, whereas the lower graphs indicate the applied voltage over time. The response of the switchable metasurface is only limited by the sensitivity and thus frame rate of the camera. In principle, even faster scan rates are possible with PEDOT to reach typical display frequencies in the region of tens of hertz.

of (a) 20 mV s^{-1}, (b) 400 mV s^{-1}, and (c) 1500 mV s^{-1}. Please note that for these measurements, we use a newly fabricated hybrid metasurface with nominally identical parameters compared to the one used for the characterization in figure 4. For all measurements in figure 5, we use linear ramps in constant cyclic phases, as shown in the lower graphs of each panel, and an exposure time of the CCD camera of 120 ms. For the slowest scan rate of 20 mV s^{-1} in figure 5(a), we find that the temporal resolution is high enough to resolve even the slightest differences in the intensity ratio I_1/I_0 of the diffracted beam I_1 and the main beam I_0. The peaks in the oxidized state (compare to figure 4(c)) are sharp and well defined and the performance of the metasurface is reproducible over several cycles with only marginal increases in the overall intensity ratio and no noticeable degradation of the PEDOT layer.

When increasing the scan rate to 400 mV s^{-1} we see in figure 5(b) that, as expected, we lose temporal resolution in

the response curve of the hybrid metasurface, which becomes even more prominent for a scan rate of 1500 mV s^{-1}. Here, we switch between oxidized and reduced states of PEDOT within 1 s, which results in a period of 2 s or a frequency of 0.5 Hz. At this scan rate, the individual data points are far spaced and become clearly visible in the intensity ratio curve. Please note that the time resolution in our experiment is set by the exposure time of the CCD camera. The individual data points in the upper panel of figure 5(c) are temporarily spaced at $\approx$ 200–300 ms, which corresponds to the sum of the exposure time of 120 ms and a short time for the software to store each individually captured image. Nevertheless, the hybrid metasurface still oscillates/cycles reproducibly between its oxidized and reduced states. Consequently, the switching speed is limited in our experiment by the sensitivity and thus exposure time and frame rate of our CCD camera and is not intrinsically limited by the switching speed of the PEDOT layer. In fact, an extension of the switching speeds of our hybrid metasurface to typical display frequencies (tens of hertz) should be possible by exchanging the cyclic voltammetry with a direct setting (step-function) of applied voltages of +0.5 V and −1 V. Furthermore, several other factors contribute to define the switching speed, which is discussed in the supplementary information.

4. Conclusion

In conclusion, we have demonstrated a novel approach for an optically active and externally and electrically switchable hybrid metasurface. We presented a unique combination of a metasurface comprising gold nanoantennas and an electropolymerized PEDOT, which allowed for electrochemically activated switchable beam steering. The feasibility of this combination for potential nanophotonic applications was demonstrated via a detailed investigation of the optical and temporal properties of the hybrid metasurface. We used Fourier-space imaging to reveal switching and diffraction angles of up to 10° with excellent conservation of the beam profiles in the first diffraction order. A temporal investigation of the intensities of the main and diffracted beams showed that we were able to actively control the efficiency of the metasurface and thus the intensity of the diffracted and primary light. We reached switching frequencies around 1 Hz, while the extension to display frequencies was only limited by the measurement components and not intrinsically by the optical and electrical properties of our hybrid metasurface. Overall, our approach holds immediate implications for the design, fabrication, and realization of optically active nanophotonic systems that are electrically switchable. Our results will help in the development of future optical technologies such as virtual and augmented reality and dynamic holography.

Acknowledgments

Conflict of interest

The authors declare no conflicts of interest.

ORCID iDs

Julian Karst ⓘ https://orcid.org/0000-0003-2422-8926
Florian Sterl ⓘ https://orcid.org/0000-0002-1025-6777
Thomas Zentgraf ⓘ https://orcid.org/0000-0002-8662-1101
Sabine Ludwigs ⓘ https://orcid.org/0000-0002-6717-8538
Mario Hentschel ⓘ https://orcid.org/0000-0002-6882-4183
Harald Giessen ⓘ https://orcid.org/0000-0002-4270-3850

References

[1] Yu N, Genevet P, Kats M, Aieta F, Tetienne J-P, Capasso F and Gaburro Z 2011 Light propagation with phase reflection and refraction *Science* **334** 333–7

[2] Sun S, He Q, Xiao S, Xu Q, Li X and Zhou L 2012 Gradient-index meta-surfaces as a bridge linking propagating waves and surface waves *Nat. Mater.* **11** 426–31

[3] Kildishev A V, Boltasseva A and Shalaev V M 2013 Planar photonics with metasurfaces *Science* **339** 1232009

[4] Arbabi A, Horie Y, Bagheri M and Faraon A 2015 Dielectric metasurfaces for complete control of phase and polarization with subwavelength spatial resolution and high transmission *Nat. Nanotechnol.* **10** 937–43

[5] Khorasaninejad M, Chen W T, Devlin R C, Oh J, Zhu A Y and Capasso F 2016 Metalenses at visible wavelengths: diffraction-limited focusing and subwavelength resolution imaging *Science* **352** 1190–4

[6] Shitrit N, Bretner I, Gorodetski Y, Kleiner V and Hasman E 2011 Optical spin hall effects in plasmonic chains *Nano Lett.* **11** 2038–42

[7] Wuttig M, Bhaskaran H and Taubner T 2017 Phase-change materials for non-volatile photonic applications *Nat. Photonics* **11** 465–76

[8] Aieta F, Genevet P, Kats M A, Yu N, Blanchard R, Gaburro Z and Capasso F 2012 Aberration-free ultrathin flat lenses and axicons at telecom wavelengths based on plasmonic metasurfaces *Nano Lett.* **12** 4932–6

[9] Yu N and Capasso F 2014 Flat optics with designer metasurfaces *Nat. Mater.* **13** 139–50

[10] Chen X, Huang L, Mühlenbernd H, Li G, Bai B, Tan Q, Jin G, Qiu C W, Zhang S and Zentgraf T 2012 Dual-polarity plasmonic metalens for visible light *Nat. Commun.* **3** 1–6

[11] Pors A, Nielsen M G and Bozhevolnyi S I 2015 Plasmonic metagratings for simultaneous determination of Stokes parameters *Optica* **2** 716

[12] Frese D, Wei Q, Wang Y, Huang L and Zentgraf T 2019 Nonreciprocal asymmetric polarization encryption by layered plasmonic metasurfaces *Nano Lett.* **19** 3976–80

[13] Mühlenbernd H, Georgi P, Pholchai N, Huang L, Li G, Zhang S and Zentgraf T 2016 Amplitude- and phase-controlled surface plasmon polariton excitation with metasurfaces *ACS Photonics* **3** 124–9

[14] Yu P, Li J, Li X, Schütz G, Hirscher M, Zhang S and Liu N 2019 Generation of switchable singular beams with dynamic metasurfaces *ACS Nano* **13** 7100–6

[15] Yu P, Li J, Zhang S, Jin Z, Schütz G, Qiu C W, Hirscher M and Liu N 2018 Dynamic janus metasurfaces in the visible spectral region *Nano Lett.* **18** 4584–9

[16] Yin X, Steinle T, Huang L, Taubner T, Wuttig M, Zentgraf T and Giessen H 2017 Beam switching and bifocal zoom lensing using active plasmonic metasurfaces *Light Sci. Appl.* **6** e17016–e17016

[17] Li J, Kamin S, Zheng G, Neubrech F, Zhang S and Liu N 2018 Addressable metasurfaces for dynamic holography and optical information encryption *Sci. Adv.* **4** eaar6768

[18] Duan X, Kamin S and Liu N 2017 Dynamic plasmonic colour display *Nat. Commun.* **8** 1–9

[19] Duan X and Liu N 2018 Scanning plasmonic color display *ACS Nano* **12** 8817–23

[20] Sterl F, Strohfeldt N, Walter R, Griessen R, Tittl A and Giessen H 2015 Magnesium as novel material for active plasmonics in the visible wavelength range *Nano Lett.* **15** 7949–55

[21] Karst J, Sterl F, Linnenbank H, Weiss T, Hentschel M and Giessen H 2020 Watching in-situ the hydrogen diffusion dynamics in magnesium on the nanoscale *Sci. Adv.* **6** eaaz0566

[22] Karst J, Hentschel M, Sterl F, Linnenbank H, Ubl M and Giessen H 2020 Optimizing magnesium thin films for optical switching applications: rules and recipes *Opt. Mater. Express* **10** 1346

[23] Duan X and Liu N 2019 Magnesium for dynamic nanoplasmonics *Acc. Chem. Res.* **52** 1979–89

[24] Liu N, Tang M L, Hentschel M, Giessen H and Alivisatos A P 2011 Nanoantenna-enhanced gas sensing in a single tailored nanofocus *Nat. Mater.* **10** 631–6

[25] Strohfeldt N, Zhao J, Tittl A and Giessen H 2015 Sensitivity engineering in direct contact palladium-gold nano-sandwich hydrogen sensors [Invited] *Opt. Mater. Express* **5** 2525

[26] Tittl A, Mai P, Taubert R, Dregely D, Liu N and Giessen H 2011 Palladium-based plasmonic perfect absorber in the visible wavelength range and its application to hydrogen sensing *Nano Lett.* **11** 4366–9

[27] Sterl F, Strohfeldt N, Both S, Herkert E, Weiss T and Giessen H 2020 Design principles for sensitivity optimization in plasmonic hydrogen sensors *ACS Sensors* **5** 917–27

[28] Strohfeldt N, Tittl A, Schäferling M, Neubrech F, Kreibig U, Griessen R and Giessen H 2014 Yttrium hydride nanoantennas for active plasmonics *Nano Lett.* **14** 1140–7

[29] Leroux Y, Lacroix J C, Fave C, Trippe G, Félidj N, Aubard J, Hohenau A and Krenn J R 2008 Tunable electrochemical switch of the optical properties of metallic nanoparticles *ACS Nano* **2** 728–32

[30] Leroux Y, Lacroix J C, Fave C, Stockhausen V, Felidj N, Grand J, Hohenau A and Krenn J R 2009 Active plasmonic devices with anisotropic optical response: a step toward active polarizer *Nano Lett.* **9** 2144–8

[31] Gholipour B, Piccinotti D, Karvounis A, Macdonald K F and Zheludev N I 2019 Reconfigurable ultraviolet and high-energy visible dielectric metamaterials *Nano Lett.* **19** 1643–8

[32] Wang Q, Rogers E T F, Gholipour B, Wang C M, Yuan G, Teng J and Zheludev N I 2016 Optically reconfigurable metasurfaces and photonic devices based on phase change materials *Nat. Photonics* **10** 60–65

[33] Gholipour B, Zhang J, MacDonald K F, Hewak D W and Zheludev N I 2013 An all-optical, non-volatile,

bidirectional, phase-change meta-switch *Adv. Mater.* **25** 3050–4

[34] Li P, Yang X, Tww M, Hanss J, Lewin M, Michel A K U, Wuttig M and Taubner T 2016 Reversible optical switching of highly confined phonon-polaritons with an ultrathin phase-change material *Nat. Mater.* **15** 870–5

[35] Komar A *et al* 2017 Electrically tunable all-dielectric optical metasurfaces based on liquid crystals *Appl. Phys. Lett.* **110** 071109

[36] Zou C, Komar A, Fasold S, Bohn J, Muravsky A A, Murauski A A, Pertsch T, Neshev D N and Staude I 2019 Electrically tunable transparent displays for visible light based on dielectric metasurfaces *ACS Photonics* **6** 1533–40

[37] Dicken M J, Aydin K, Pryce I M, Sweatlock L A, Boyd E M, Walavalkar S, Ma J and Atwater H A 2009 Frequency tunable near-infrared metamaterials based on VO$_2$ phase transition *Opt. Express* **17** 18330

[38] Briggs R M, Pryce I M and Atwater H A 2010 Compact silicon photonic waveguide modulator based on the vanadium dioxide metal-insulator phase transition *Opt. Express* **18** 11192

[39] Stockhausen V, Martin P, Ghilane J, Leroux Y, Randriamahazaka H, Grand J, Felidj N and Lacroix J C 2010 Giant plasmon resonance shift using poly(3,4-ethylenedioxythiophene) electrochemical switching *J. Am. Chem. Soc.* **132** 10224–6

[40] Zhang S, Feng L, Zhang H, Liu M and Xu T 2020 Electrochromic modulation of plasmonic resonance in a PEDOT-coated nanodisk metasurface *Opt. Mater. Express* **10** 1053

[41] Yakubovsky D I, Arsenin A V, Stebunov Y V, Fedyanin D Y and Volkov V S 2017 Optical constants and structural properties of thin gold films *Opt. Express* **25** 25574

[42] Huang L, Chen X, Mühlenbernd H, Li G, Bai B, Tan Q, Jin G, Zentgraf T and Zhang S 2012 Dispersionless phase discontinuities for controlling light propagation *Nano Lett.* **12** 5750–5

[43] Wieland M, Malacrida C, Yu Q, Schlewitz C, Scapinello L, Penoni A and Ludwigs S 2020 Conductance and spectroscopic mapping of EDOT polymer films upon electrochemical doping *Flex. Print. Electron.* **5** 014016

[44] Heinze J, Frontana-Uribe B A and Ludwigs S 2010 Electrochemistry of conducting polymers-persistent models and new concepts *Chem. Rev.* **110** 4724–71

[45] Baba A, Lübben J, Tamada K and Knoll W 2003 Optical properties of ultrathin poly(3,4-ethylenedioxythiophene) films at several doping levels studied by in situ electrochemical surface plasmon resonance spectroscopy *Langmuir* **19** 9058–64

[46] Kurvits J A, Jiang M and Zia R 2015 Comparative analysis of imaging configurations and objectives for Fourier microscopy *J. Opt. Soc. Am.* A **32** 2082

[47] Komar A, Paniagua-Domínguez R, Miroshnichenko A, Yu Y F, Kivshar Y S, Kuznetsov A I and Neshev D 2018 Dynamic beam switching by liquid crystal tunable dielectric metasurfaces *ACS Photonics* **5** 1742–8